https://doi.org/10.2352/ISSN.2169-2629.2017.32.300

Scene Color Correction Under Non-Uniform Spatial Illumination and Atmospheric Transmittance

Hiroaki Kotera; Kotera Imaging Laboratory, Chiba, Japan

Abstract

Our daily scene visibility is degraded due to both spatial non-uniformities in **A) *illumination*** *and* **B) *atmospheric transmittance***. *Since the illumination extremely drops in the shade of tree or house and the atmospheric transmittance is disturbed by floating particles in the air, we never see the grand truth scenes even if under clear sky. This paper challenges to recover the scene color visibilities by removing the spatial non-uniformities of* **A)** *and* **B)**.

Firstly, a modified BLF-SSR (Bi-Lateral Filter Single-Scale Retinex) is introduced to enhance the shadow visibility. A sharp bilateral filter is used for creating the edge-preserving surround to make a "halo-less" SSR like as MSR (Multi-Scale Retinex).

Secondly, an ***improved*** de-hazing algorithm is proposed to estimate the *scene transmittance based on dark channel prior hypothesis. The proposed* single image de-hazing algorithm *works* ***to remove the disturbances caused by atmospheric layer*** *and to see the haze-free objects through the air pollution. The model works not only for heavy air pollution but also for thin ha scenes often encounters in daily life.*

The proposed dehazing model shows "veiling factor α" is a key parameter for improving the usual scene's color appearance. The veiling factor is set to $\alpha \cong 0.9$ for heavy PM 2.5 pollution scene, while it should be set relatively lower values such as $\alpha \cong 0.7 \sim 0.2$ for the daily thin hazy scene. Once estimated scene transmittance is used to preset the veiling factor automatically.

The paper introduces typical cases where Retinex and De-hazing work collaborative and complementary in comparison with state-of-the art other models.

Introduction

Electronic camera is hard to catch the details in the shade of tree or house, while human vision can do. "***Retinex"*** is a roots of vision model developed by Land and McCann[1] which restores the scene reflectance not by "*pixel-to-pixel*" but by "*spatial-to-pixel*" process like as human vision. *Retinex* traced a long history [2][3]. Jobson et al [4], and many others have advanced the Single-Scale Retinex (***SSR***) into Multi-Scale Retinex (***MSR***) based on the concept of Center/ Surround (*C/S*). Since the weights for creating MSR as an integrated sum of SSRs have been decided empirically, the author clarified the statistical weighting rule in the "*adaptive scale-gain*" ***ASG-MSR*** [5][6]. Though ASG-MSR works stable and robust, it has a drawback of high computation cost. The paper introduces the modified SSR as an alternative to ASG-MSR.

Recently, air pollution by PM2.5 becomes a serious problem at China and its neighbors. The de-hazing task also has been a long-pending question at NASA Langley Research Center. NASA advanced their MSR to a novel system called Visual Servo [7] for manipulating dense foggy aerial scenes and HDR cosmic images. While, different from NASA's approach, the mainstream in current de-hazing model is based on the atmospheric scattering physics. Basic theory by McCartney [8] evolved into practical single-image models by Fattal [9], Tan [10], Tarel [11], and Yu [12] etc. Above all, the Dark Channel Prior (DCP) model by He *et al*.[13] has been most attractive due to its high performance. Many papers followed DCP as reviewed in the survey report by S. Lee [14].

The key to unveiling the disturbance by air pollution is how to estimate the smooth transmission (depth) map. The author [15][16] improved He's DCP process for estimating a banding-free depth map with anisotropic filtering. The model was applied to sharpen foreground and/or background separated by the depth map [17].
A depth-based contrast enhancement by Galdran *et al*. [18] is also noteworthy as a variational framework. Another notable approach is a multi-scale STRESS model by Dravo and Herdeberg [19].

So far these de-hazing tasks mainly aimed at unveiling a dense fog, mist, or heavy PM 2.5 pollution. Though, we never see the grand truth haze-less scenes even under clear sky, because any floating particles degrade the scene visibility. Different from the common objective, this paper presents a joint *Retinex-Dehazing* model, which is intentionally applied to color correction even for daily thin hazy scenes. The idea coping with Retinex is not new, as reported by Xie *et al*. [20] or Wang and Xu [21]. Xie model substitutes the MSR on luminance component for the depth map, where the luminance MSR is adjusted to be similar to the DCP-based depth map. The idea looks tricky and illogical. While, Wang model applies a small-scale SSR to the far region and a large-scale SSR to the near region in the DCP-based depth map. This idea is simple and practical, but the effects are Retinex itself.

The proposed model is designed for Retinex and Dehazing working independent but collaborative as illustrated in Figure 1. The 1st stage *Retinex* corrects the single camera image just taken as under uniform illumination and the 2nd stage *Dehazing* removes the disturbance caused by passing through the atmospheric pollution layer. The model demonstrates how the joint sequential processes work collaborative to remove the ***two spatial non- uniformities***, first in ***illumination*** and second in ***atmospheric transmittance*** according to the two steps sequential processes by

$$\boldsymbol{O}(x,y)=\boldsymbol{Dehaze}\left\{\boldsymbol{Retinex}\left\{\boldsymbol{I}(x,y)\right\}\right\}\ ;\ \text{output image} \qquad (1)$$

The order of two stages may be changed, but the result is not the same. ***Retinex*** is used for a pre-processor as needed.

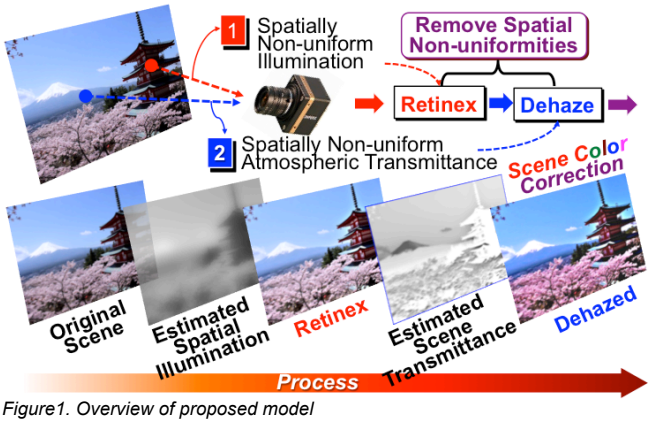

Figure1. Overview of proposed model

Removal of Spatial Non-uniformity in Illumination

SSR, ASG-MSR, and Halo-less BLF-SSR

A camera image $\boldsymbol{I}(x, y)$ from the scene with reflectance $R(x, y)$ under the illumination $L(x, y)$ is simply given by

$$\boldsymbol{I}(x,y) = \boldsymbol{L}(x,y)\boldsymbol{R}(x,y) \tag{2}$$

The major objective of Retinex is to restore the scene reflectance $\boldsymbol{R}(x, y)$ under unknown illumination $\boldsymbol{L}(x, y)$.

[SSR]

In the basic ***SSR***, the reflectance $\boldsymbol{R}(x, y)$ is restored by assuming that the spatial average $\boldsymbol{S}_m(x, y)$ of input $\boldsymbol{I}(x, y)$ reflects the scene illumination $\boldsymbol{L}(x, y)$ as follows.

$$\begin{aligned} &\boldsymbol{R}_i(x,y)^m_{SSR} = \frac{\boldsymbol{I}_i(x,y)}{\boldsymbol{L}(x,y)} \cong \frac{\boldsymbol{I}_i(x,y)}{\boldsymbol{S}_m(x,y)}; \\ &\boldsymbol{S}_m(x,y) = \left\langle G_m(x,y) * \boldsymbol{I}_i(x,y) \right\rangle \\ &i = R,G,B; \quad G_m = K\exp\left\{-\left(x^2+y^2\right)/\sigma_m^2\right\}; \\ &\iint G_m dxdy = 1; \quad \langle * \rangle = Convolution \end{aligned} \tag{3}$$

Surround $\boldsymbol{S}_m(x, y)$ is given by the convolution of $\boldsymbol{I}(x, y)$ and Gaussian function $G_m(x, y)$ with standard deviation σ_m.

[ASG-MSR: Adaptive Scale-Gain MSR]

Since ***SSR*** with single kernel size of $\boldsymbol{G}_m(x, y)$ causes a banding artifact such as "*halo*" on the boundary between light and shade, ***MSR*** is mostly used in practice.

MSR is composed of weighted sum of ***SSR***s with different scale σ_m as given by

$$\boldsymbol{R}_i(x,y)_{MSR} = \sum_{m=1}^{M} W_m \boldsymbol{R}_i(x,y)^m_{SSR} \tag{4}$$

Though the conventional ***MSR*** used a constant weight W_m derived empirically, ***ASG-MSR*** [6] claimed a clear decision rule for W_m dependent to scale σ_m and adaptive to given image as follows.

$$\begin{aligned} &\boldsymbol{R}_i(x,y)_{ASG-MSR} = C\sum_{m=1}^{M} W(\sigma_m)\left\{\frac{\boldsymbol{I}_i(x,y)}{\boldsymbol{S}_m(x,y)}\right\} \\ &W(\sigma_m) = \left\{\Sigma_{C/S}(\sigma_m) \Big/ \sum_{m=1}^{M} \Sigma_{C/S}(\sigma_m)\right\} \\ &C = range\ adjust\ constant \cong 1/3\ (default) \\ &\Sigma_{C/S}(\sigma_m) = \left\{\frac{1}{XY}\sum_{x=1}^{X}\sum_{y=1}^{Y}\left[Y_{SSR}(x,y) - Ave\left\{Y_{SSR}(x,y)\right\}\right]^2\right\}^{1/2} \\ &Y_{SSR}(x,y) = Y(x,y)/S_m(x,y)\ : SSR\ for\ Luminance\ Y \end{aligned} \tag{5}$$

Here, $\Sigma_{C/S}(\sigma_m)$ denotes the standard deviation measured for each SSR of Luminance, $Y_{SSR}(x, y)$ with scale σ_m. The weight $W(\sigma_m)$ is given by the ratio of each $\Sigma_{C/S}(\sigma_m)$ vs. total sum $\underset{m=1\sim M}{Sum}\left\{\Sigma_{C/S}(\sigma_m)\right\}$.

Note that $W(\sigma_m)$ reflects an index how the *Retinex* effects are distributed to each ***SSR*** with scale σ_m.

[Halo-less BLF-SSR]

A fatal drawback in SSR with Gaussian surround lies in "*halo*" artifact caused by the slow gradient of surround $\boldsymbol{S}_m$ across the boundary of light and shade, because $\boldsymbol{S}_m$ works as the denominator in Eq. (2). To create a *halo-less* ***SSR***, *Bilateral filter* (***BLF***) is introduced to generate the luminance surround $\boldsymbol{S}_{BLF}$ as given by

$$\begin{aligned} \boldsymbol{S}(\boldsymbol{q},\sigma_S,\sigma_R)_{BLF} &= BilateralFilter\left\{Y(x,y)\right\} \\ &= \frac{1}{W}\sum_{\boldsymbol{p}\subset\Omega(\boldsymbol{q})} G_S\left(\|\boldsymbol{p}-\boldsymbol{q}\|\right) G_R\left(Y(\boldsymbol{p}) - Y(\boldsymbol{q})\right) \end{aligned} \tag{6}$$

BLF is composed of a couple of two *Gaussian filters* $\boldsymbol{G}_S$ and $\boldsymbol{G}_R$. $\boldsymbol{G}_S$ works as a spatial filter to smooth $Y(\boldsymbol{q})$; $\boldsymbol{q}=(x, y)$ for the neighboring pixels in $\boldsymbol{p}\subset\Omega(\boldsymbol{q})$ with standard deviation σ_S. While, $\boldsymbol{G}_R$ works as an edge-preserving range filter with intensity deviation parameter σ_R to suppress the smoothing for the pixels with high intensity gradient in the edge area.

The key point of proposed *halo-less* ***SSR*** is to use a very sharp range filter $\boldsymbol{G}_R$ with $\sigma_R << \sigma_S$. Applying the new surround $\mathbf{S}_{BLF}$ to the basic ***SSR*** in Eq. (3), a *halo-less* ***BLF-SSR*** is constructed as

$$\boldsymbol{R}_i(x,y)_{BLF\text{-}SSR} = \frac{\boldsymbol{I}_i(x,y)}{\boldsymbol{L}(x,y)} \cong \frac{\boldsymbol{I}_i(x,y)}{\boldsymbol{S}(x,y,\sigma_S,\sigma_R)_{BLF}} \tag{7}$$

Figure 2 illustrates ***BLF-SSR*** as an alternative to ***ASG- MSR***.

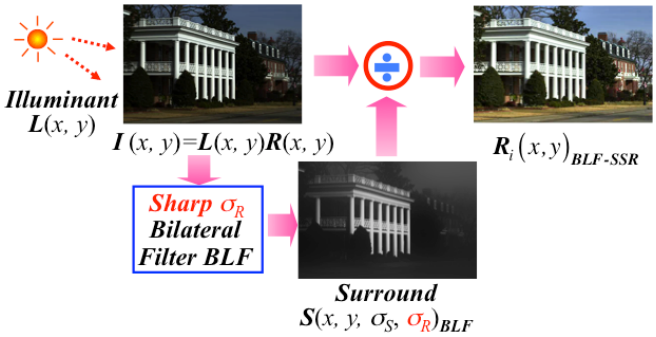

Figure 2. Halo-less BLF-SSR as an alternative to ASG-MSR

In the proposed ***BLF-SSR***, the new surround $\boldsymbol{S}_{BLF}$ created from the luminance channel Y with sharp ***BLF*** is commonly used for all channels of i=*R, G, B*.

Figure 3 compares the performances on the boundary of light and shade. It's shown that the *halo-less* ***BLF-SSR*** works better than *basic* ***SSR*** and close to ***ASG-MSR*** with its reduced halo artifacts.

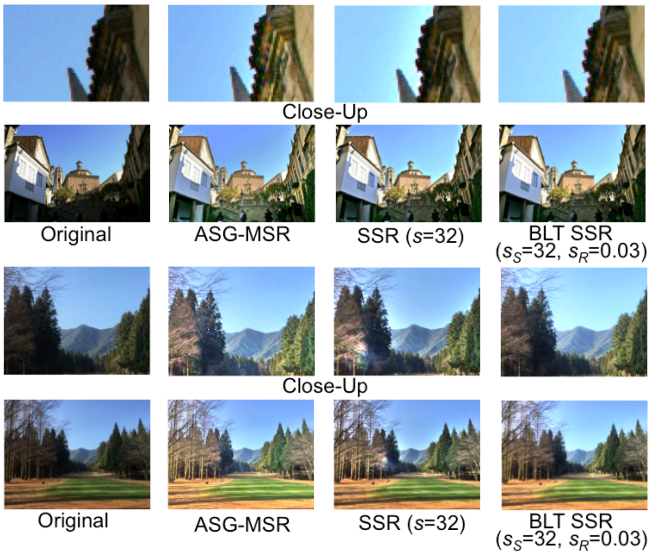

Figure 3. "Halo" comparisons in three types of Retinex

Removal of Spatial Non-uniformity in Atmospheric Transmittance

Improved Single Image Dehazing Algorithm

The requirements for solving the ill-posed dehazing problem are summarized on the following two points.

[1] Extraction of *skylight* as a scene illumination

[2] Estimation of *transmission map*

The author[15] improved He's DCP process by the method of

- *Skylight* detection from local minimum in *luminance Y* not *RGB*.
- *Transmission map refining* by *an isotropic smoothing filter* as a substitute for troublesome *soft-matting process*

Figure 4 illustrates the composition of camera image through any floating particles based on atmospheric scattering physics.

The objective is to restore the albedo $\boldsymbol{\rho}$ or radiance $\boldsymbol{J}$ of haze-less scene by unveiling the scattered *airlight* from a single camera image I.

The hazed camera image $\boldsymbol{I}(z)$ is composed of the two terms as

$$\boldsymbol{I}(z) = \boldsymbol{J}(z)\boldsymbol{t}(z) + \boldsymbol{A}(1\text{-}\boldsymbol{t}(z)) \quad \textit{where, } \boldsymbol{J}(z) = \boldsymbol{A}\boldsymbol{\rho}(z),\ \boldsymbol{t}(z) = exp^{-\beta d(z)} \tag{8}$$

The 1st term denotes the direct transmission image from the scenic objects and the 2nd term means the *airlight* scattered from the *skylight* $\boldsymbol{A}$. The *skylight* $\boldsymbol{A}$ acts as a scene illumination and the *airlight* causes the hazy scene by veiling the direct transmission image. $\boldsymbol{J}(z)$ and $\boldsymbol{\rho}(z)$ denote the scene ***radiance*** and ***albedo***. The scene transmittance $\boldsymbol{t}(z)$ is attenuated exponentially according to the scene depth $d(z)$ with scattering coefficient $\beta(\lambda)$. Since the ***Mie*** *scattering* is dominant for floating particles with larger size than wavelength such as PM2.5 or mist, the scattering coefficient is assumed to be a constant $\beta(\lambda)\cong\beta$ independent of wavelength. Here, note that $z=(x, y)$ denotes each pixel coordinates in the 2-D camera image $\boldsymbol{I}(z)$ captured from the objects at scene depth $d(z)$.

Now the scattered flux $d\boldsymbol{F}$ from the floating particles with a small volume dV at distance r is given by

$$d\boldsymbol{F}(r,\lambda) = \boldsymbol{k}\beta(\lambda)dV,\ dV = r^2 dr d\omega \tag{9}$$

Where, $\boldsymbol{k}$ means the illuminant and $d\omega$ denotes a solid angle. Hence, the irradiance change $d\boldsymbol{E}$ by $d\boldsymbol{F}$ is described as

$$d\boldsymbol{E}(r,\lambda) = d\boldsymbol{F}(r,\lambda)e^{-\beta(\lambda)r} / r^2 \tag{10}$$

The increase $d\boldsymbol{L}$ in radiance $\boldsymbol{L}$ is calculated as

$$d\boldsymbol{L}(r,\lambda) = d\boldsymbol{E}(r,\lambda) / d\omega = \boldsymbol{k}\beta(\lambda)e^{-\beta(\lambda)r}dr \tag{11}$$

Thus the accumulated scattering between r=0 (camera) and r=d (object) denotes the *airlight* radiance, that is

$$\boldsymbol{L}(d,\lambda) = \int_0^d d\boldsymbol{L}(r,\lambda)dr = \boldsymbol{k}\left(1 - e^{-\beta(\lambda)d}\right) \tag{12}$$

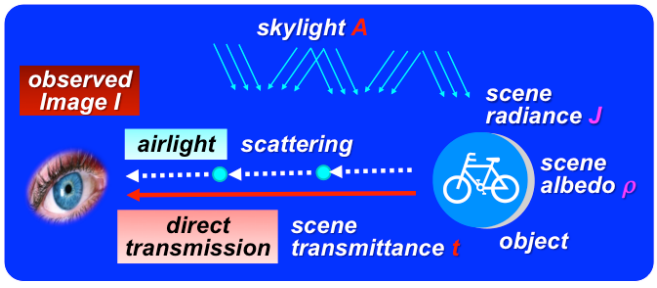

Figure 4. Hazy Image caused by Atmospheric Scattering

Since Eq. (12) denotes a monotonously increasing function, the *airlight* is more amplified as taking the longer path.

Letting the *airlight* radiance be $\boldsymbol{L}_\infty(\lambda)$ at d=∞, Eq. (12) is simply described for Mie scattering with $\beta(\lambda)\cong\beta$ as

$$\boldsymbol{L}(d,\lambda) = \boldsymbol{L}_\infty(\lambda)\left(1 - e^{-\beta d}\right) \tag{13}$$

Now, the *skylight* is assumed to be $\boldsymbol{A}$=$\boldsymbol{k}\cong\boldsymbol{L}_\infty(\lambda)$ corresponding to the *airlight* radiance at infinite distance.

Skylight Detection

To estimate the *skylight* $\boldsymbol{A}$, He et al. performed DCP operation on $\boldsymbol{I}(z)$, which selects the darkest channel in *RGB* and replaces the pixels' values by the lowest in a local minimum filtered area $\boldsymbol{\Omega}(z)$.

$$\boldsymbol{I}^{dark}(z) = \min_{\boldsymbol{w}\in\boldsymbol{\Omega}(z)}\left[\min_{C\in\{R,G,B\}} I^C(\boldsymbol{w})\right] \tag{14}$$

As a result, the 1st $\boldsymbol{J}$ term in Eq. (8) approaches to zero.

$$J^{dark}(z) = \min_{\boldsymbol{w}\in\boldsymbol{\Omega}(z)}\left[\min_{C\in\{R,G,B\}} J^C(\boldsymbol{w})\right] \to 0 \tag{15}$$

This DCP hypothesis is supported by many observation data, hence only the 2nd term is remained as

$$I^{dark}(z) \cong \min_{\boldsymbol{w}\in\boldsymbol{\Omega}(z)}\left[\min_{C\in\{R,G,B\}} A^C\{1\text{-}t(\boldsymbol{w})\}\right] \tag{16}$$

Since the transmittance $\boldsymbol{t}(z)$ goes to zero at d=∞, we get

$$I^{dark}(z)_{d=\infty} \cong \min_{\boldsymbol{w}\in\boldsymbol{\Omega}(z)}\left[\min_{C\in\{R,G,B\}} A^C\right] \tag{17}$$

Since the *skylight* $\boldsymbol{A}$ equals the *airlight* coming from infinite d=∞, He et al obtained $\boldsymbol{A}$ by finding the brightest area in $I^{dark}(z)_{d=\infty}$.

Different from the He's, the proposed model applied DCP process only on the luminance channel $Y(z)$. Applying a local minimum filter to the luminance $Y(z)$ without taking the dark channel of *RGB*, we get

$$Y^{dark}(z) = \min_{\boldsymbol{w}\in\boldsymbol{\Omega}(z)} Y(\boldsymbol{w}) \tag{18}$$

Thinking the local minimum in the dark channel must be reflected to the local minimum of $Y(z)$, the *skylight* $\boldsymbol{A}$ may be estimated by extracting the brighter area Ω_{Sky} and taking the average as

$$\tilde{\boldsymbol{A}} = \operatorname*{mean}_{\boldsymbol{w}\in\Omega_{Sky}(z)}\{\boldsymbol{I}(\boldsymbol{w})\}\ for\ \Omega_{Sky}(z) = area\{Y^{dark}(z) \ge Y_H\} \tag{19}$$

This simplified method proved to be comparable to that by He et al as shown in Figure 5. Though the proposed method has a tendency to detect a little bit larger area as a *skylight* than that by He et al, its positions and colors are much the same.

Rough Estimation of Scene Transmittance

Normalizing Eq. (8) by the estimated *skylight* $\tilde{\boldsymbol{A}}$, it's eliminated from the 2nd term as

$$I^C_{Norm}(z) = \frac{I^C(z)}{\tilde{A}^C} = \frac{J^C(z)}{\tilde{A}^C}t(z) + (1\text{-}t(z))\ for\ C = R,G,B \tag{20}$$

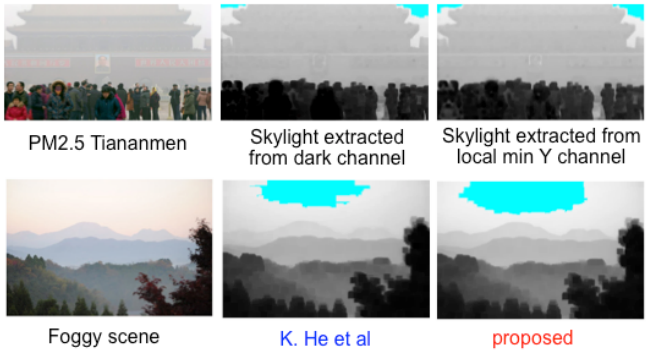

Figure 5. Luminance-based Skylight Detection

He et al applied DCP to Eq. (20) again. As well, the 1st term goes to zero and the 2nd term is remained. Hence the scene transmittance is estimated as

$$\tilde{t}(z)_{He}^{rough} \cong 1-\left[I_{Norm}^{C}(z)\right]^{dark} = 1-\min_{w\in\Omega(z)}\left[\min_{C\in\{R,G,B\}}\frac{I^{C}(w)}{A^{C}}\right] \quad (21)$$

Since the local minimum filter in Eq. (22) leads to a fatal banding artifact, the proposed model omitted this and estimated as

$$\tilde{t}(z)_{proposed}^{rough} \cong 1-\left\{\min_{C\in\{R,G,B\}}\frac{I^{C}(z)}{A^{C}}\right\} \quad (22)$$

Once the *skylight* $\boldsymbol{A}$ and *scene transmittance* $\boldsymbol{t}(z)$ are estimated, the scene *albedo* is recovered from Eq. (8) as

$$\tilde{\rho}(z) \cong \tilde{J}(z)/\tilde{A} = \left(I(z)/\tilde{A}-1+\tilde{t}(z)\right)/Max\left[\tilde{t}(z), t_0\right] \quad (23)$$

Where, *Max* [,] is a limiter to take $\tilde{t}(z) \geq t_0$ at very low transmit -tance pixel point for the *albedo* $\tilde{\rho}(z)$ not to diverge.

Now, Figure 6 shows the scene *albedo* $\tilde{\rho}(z)$ unveiled with

[1] $\tilde{t}(z)_{He}^{rough}$ and [2] $\tilde{t}(z)_{proposed}^{rough}$.

Comparing both, a heavy banding artifact appears in (c) by He et al caused by the local minimum filter, while disappears in (d) by the proposed model. However, looking carefully, the back signboard or front people in (c) look clear than (d). That is, both have their own drawbacks. Since the scene transmittance $\boldsymbol{t}(z)$ reflects a depth map, it should be flat for the objects located at the same distance. But, the estimated $\tilde{t}(z)_{proposed}^{rough}$ in (a) looks irregular than $\tilde{t}(z)_{He}^{rough}$ in (b). This irregularity is the drawback in proposed model and the reason why the sharpness is lost in Figure 6 (d).

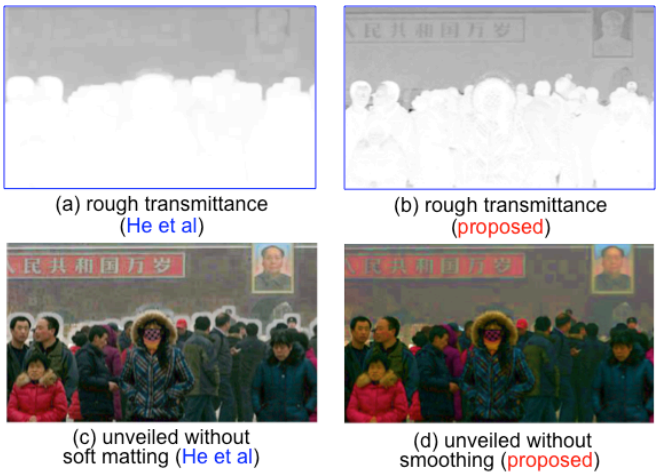

Figure 6. Problems in rough estimated scene transmittance

Refining Scene Transmittance

Since popular *Gaussian filter* causes banding artifact by edge blurring, two *edge-preserving smoothing filters* are examined:

[A] *Perona-Malik* (***PM***) *filter* [B] *Bilateral* (***BL***) *filter*

Perona-Malik filter [22] is based on anisotropic thermal diffusion. The scale-space diffusion across the edges in the scene transmittance $\boldsymbol{t}(\mathbf{z}, t)$ is suppressed according to

$$\begin{aligned}\partial \boldsymbol{t}(z,\tau)/\partial\tau &= div\left[c(z,\tau)\nabla \boldsymbol{t}(z,\tau)\right] \\ &= c(z,\tau)\Delta \boldsymbol{t}(z,\tau)+\nabla c(z,\tau)\nabla \boldsymbol{t}(z,\tau)\end{aligned} \quad (24)$$

Where, the operators denote *div* =*Divergence*, $\nabla = (\partial/\partial x, \partial/\partial y) = Gradient$, $\Delta = \left(\partial^2/\partial x^2, \partial^2/\partial y^2\right) = Laplacian$, $c(z,\tau)$ and τ denote a thermal diffusion coefficient and the passage of time as a scale parameter.

On the other hand, *Bilateral filter* [23] is composed of a couple of two *Gaussian* filters, one used for spatial smoothing and another for edge preserving as given by

$$\tilde{t}(q,\sigma_S,\sigma_R)^{BL} = \frac{1}{W}\sum_{p\subseteq\Omega(q)} G_S\left(\|p-q\|\right)G_R\left(\tilde{t}(p)-\tilde{t}(q)\right) \quad (25)$$

$\boldsymbol{G_S}$ works as a spatial filter to smooth $\boldsymbol{t}(z,\tau)$ for the neighboring pixels in $p\subset\Omega(q)$ with standard deviation σ_S. While, $\boldsymbol{G_R}$ suppresses the smoothing for the pixels with high intensity gradient in the edge area by smaller σ_R than σ_S. The smoothing parameters (τ, *k*, σ) for ***PM*** (τ, *k*, σ) and (σ_S, σ_R) for ***BL*** (σ_S, σ_R) filters are set adaptive to the gradient of *scene transmittance*.

Figure 7 shows how the *PM* and *BL* filters work effective.

The de-hazing method is useful not only for a heavy polluted scene but also for usual camera images even if taken under clear sky. Since a degraded image passing through the floating particles is veiled with the *airlight* given by the 2nd term in Eq. (8), the haze-less grand truth scene color may be recovered by unveiling the scattered *airlight*.

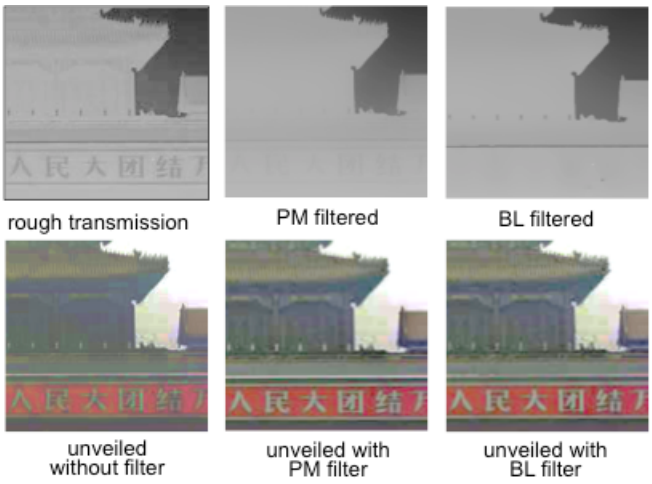

Figure 7. Smoothing effects in scene transmittance

Veiling Factor and Its Automatic Tuning

Now, the degree of *airlight* mixed with direct transmission light must be so high for heavy air pollution such as PM 2.5 at Beijing, but may be rather low for daily thin foggy or misty scenes.

Here, a veiling factor α is newly introduced to limit the *scene transmittance* in Eq. (22) with $0 < \alpha < 1$ as

$$\tilde{t}(z)^{rough}_{proposed} \cong 1\text{-}\alpha \left\{ \min_{C\in\{R,G,B\}} \frac{I^C(y)}{A^C} \right\} \quad (26)$$

In practice, the veiling factor is set to high value $\alpha \cong 0.9$ for heavy pollution, while to the lower value $\alpha \cong 0.5\sim0.2$ for thin pollution. *Figure* 8 shows the typical de-hazed results by manual tuning of the veiling factors.

Though the optimal tuning of veiling factor is a hard task, we examined the following idea to estimate a reasonable α as

$$\hat{\alpha} \cong 1 - mean\left[\tilde{t}(z)^{smooth}\right] = 1 - \frac{1}{XY}\sum_{x=1,y=1}^{x=X,y=Y} \tilde{t}(x,y)^{smooth} \quad (27)$$

This idea reuses the once estimated scene transmittance and α is approximated by subtracting the average transmittance from 1.0.

De-Hazing Coping with Retinex

Which is effective Retinex or Dehazing ?

Retinex and *Dehazing* developed independently with their different objectives each other, but have a common purpose to recover the degraded scene visibilities by removing the spatial non-uniformity. Both methods have their advantages. *Retinex* is very good at enhancing the local shadow visibility in the scenes placed under the intense shade and light. While, *Dehazing* works well to correct the color appearance by unveiling the scattered *airlight* that covers whole scene.

Figure 9 shows typical samples *Retinex* and *Dehazing* claims their merits each other. Generally, the *proposed BLF-SSR* as well as *ASG-MSR,* is widely applied to the scenes with intense shade and light. On the other hand, the proposed *De-hazing algorithm* doesn't have any criterion for tuning the optimal veiling factor at present. In Figure 9 (a), the *De-hazing* task resulted in little or no effect even tuning the parameter α, because this scene may be mainly degraded not by the *airlight* but by the non-uniform spatial illumination.

Figure 8. De-hazed samples by tuning veiling factor α

Figure 9. Which is effective Retinex or De-hazing

Automatic Color Correction for Daily Scenes

The final goal of this paper is to restore the scene colors degraded by the spatial non-uniformities in both of illumination and atmospheric transmittance. It's a lot of fun how the synergies are gained by the collaboration of *Retinex* and *Dehazing*.

Figure 10 shows the collaboration samples applied to daily scenes influenced by the spatial non-uniformities in both of Illumination and atmospheric transmission. According to Eq. (1), we applied the two-stage processing, *BLF-SSR* first and *Dehazing* next. All processes are performed in full automatic. In the second *Dehazing* stage, the veiling factor α is estimated automatically using Eq. (27).

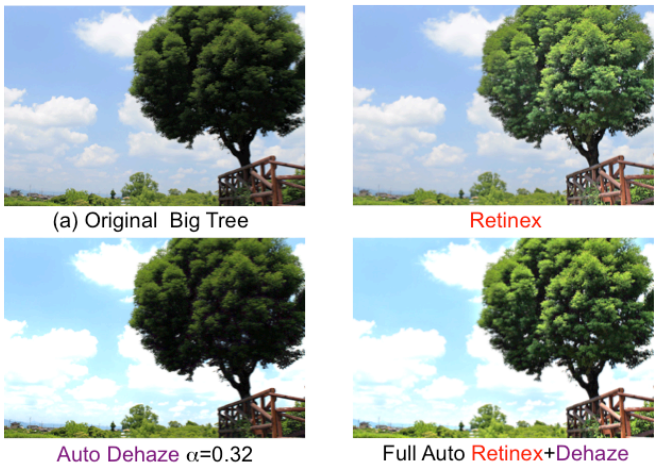

Figure 10 (a). De-hazing effects by collaboration with Retinex

Figure 10 (b). *De-hazing effects by collaboration with Retinex*

Comparison with Up-To-Date Dehazing Models

Lastly, the proposed model is compared with typical up-to-date dehazing models as collected in Figure 11. Individuality in each model appears scene-to-scene. Galdran in (a) is very good, while, the proposed model dramatically made visible the Tower in (b). Dravo and Hardeberg in (c) and (d) are excellent, though, the shadow visibility and greenish colors are better improved by the proposal coping with Retinex. Wang and Xu in (e) and (f) show the depth-dependent *SSR* effects, while the proposed model resulted in the better *dehazing* coping with *BLF-SSR*.

Conclusions

The paper proposed a scene color correction strategy by paying our attention to the spatial non-uniformities in illumination and atmospheric transmittance. Both non-uniformities in our daily viewing scenes prevent the true color reproduction. A two-stage model coupled with *Retinex* and *Dehazing* worked with synergetic effects to restore the degraded scene colors. While, the model has a drawback hard to reproduce an object such as floating clouds confusing with haze or mist. Further research for estimating more reliable veiling factor is left behind as a future work.

References

[1] E. H. Land and J. J. McCann, J. Opt. Soc. Am., 61, 1–11,1971.
[2] J. J. McCann, "Retnex at 40", J. E. I., 13(1) 6-145, 2004.
[3] J. J. McCann, "Retnex at 50", Workshop, EI2016, 2016.
[4] D. Jobson et al, IEEE Trans., Image Proc., 6, 451-462, 1997.
[5] H. Kotera and M. Fujita, Proc. CIC10, 166-171, 2002.
[6] M. Yoda and H. Kotera, Proc. NIP20, 660-663, 2004.
[7] G. Woodell et al, Proc. SPIE 6246, 2006
[8] S. Narasimhan, Jour. Comp. Vision, 48(3), 233-254, 2002.
[9] R. Fattal: Proc. ACM SIGGRAPH, 27, 1-9, 2008.
[10] R. Tan: Proc. IEEE CVPR, 1-8, 2008.
[11] J. Tarel and N. Hautiere: Proc. ICCV 2201-2208, 2009.
[12] J. Yu et al., Proc. ICSP, 1048-1052, 2010.
[13] K. He et al., Proc. IEEE CVPR, 1956-1963, 2009.
[14] S. Lee et al., EURASIP, J. Image and Video Processing, 2016
[15] H. Kotera, Proc. CIC22, 59-64, 2014
[16] H. Kotera, Proc. IEVC 2014, Samui, 4B-4, 2014.
[17] H. Kotera, Proc. 1st ICAI, Tokyo, T-101-02, 2015.
[18] A. Galdran et al., European Conf. Computer Vision Workshop, 2014.
[19] V. J. W. Dravo and J. Y. Herdeberg, Jour. IS&T., 60(1), 2016
[20] B. Xie et al., Proc. Intl. Conf. Intel. Sys. Des. Eng. Appl., 848-, 2010.
[21] W. Wang and L. Xu, Intl. J. Hybrid Info. Tech., 7, 353-364, 2014.
[22] P. Perona and J. Malik: IEEE Trans, PAMI, 12,7, 629-639, 1990.
[23] C. Tomasi and R. Manduchi: Proc. 6th IEEE ICCV, 839-, 1998.

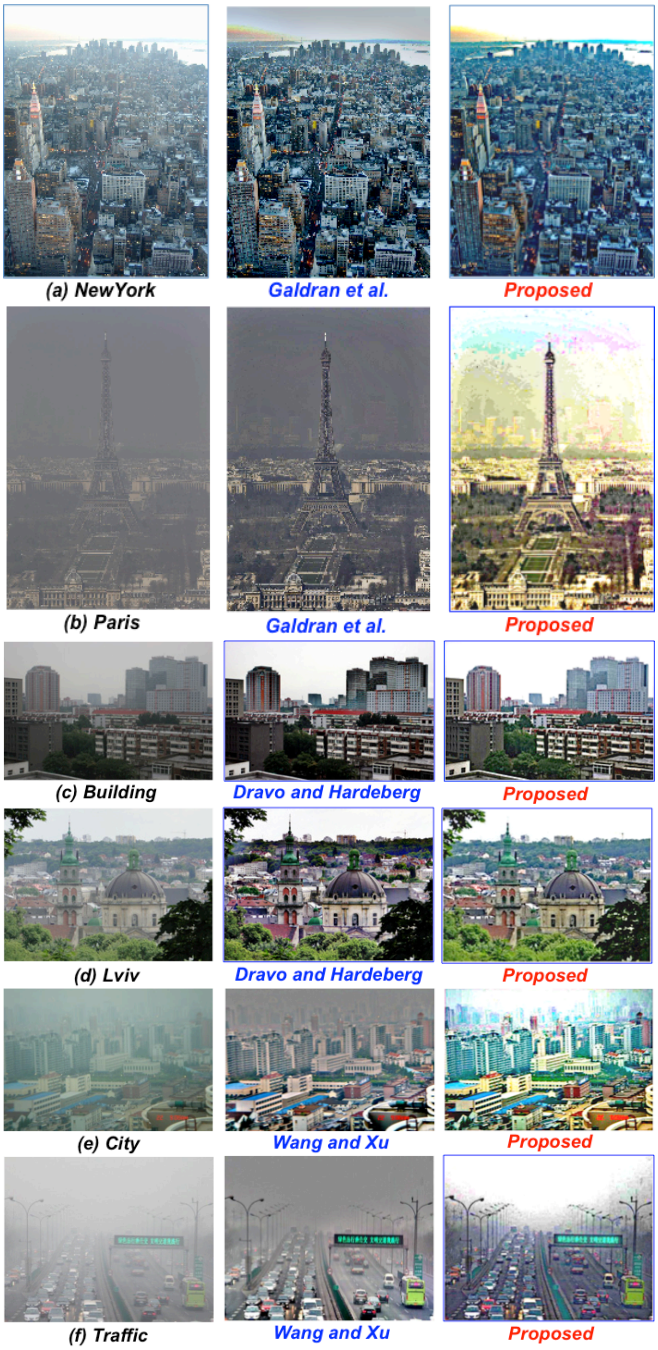

Figure 11. Comparison with up-to-date typical methods

Author Biography

Hiroaki Kotera *joined Panasonic in 1963. He received PhD from Univ. of Tokyo. After worked at Matsushita Res. Inst. Tokyo during 1973-1996, he was a professor at Chiba University. He retired in 2006 and is collaborating with Chiba University. He received 1993 IS&T honorable mention, 1995 SID Gutenberg prize, 2005 IEEE Chester Sall award, 2007 IS&T Raymond. C. Bowman award, 2009 SPSTJ and 2012 IIEEJ best paper awards. He is a Fellow of IS&T and IIEEJ.*